Energy & Environmental Science

Identifying geologic characteristics and operational decisions to meet global carbon sequestration goals

Journal:	*Energy & Environmental Science*
Manuscript ID	EE-ART-08-2020-002488.R1
Article Type:	Paper
Date Submitted by the Author:	23-Sep-2020
Complete List of Authors:	Middleton, Richard; Los Alamos National Laboratory, Earth and Environmental Sciences Ogland-Hand, Jonathan; ETH Zürich, Department of Earth Sciences Chen, Bailian; Los Alamos National Laboratory, Earth and Environmental Sciences Bielicki, Jeffrey; The Ohio State University, Department of Civil, Environmental, and Geodetic Engineering and John Glenn College of Public Affairs; The Ohio State University, John Glenn College of Public Affairs Ellett, Kevin; Indiana University Bloomington, Indiana Geological and Water Survey Harp, Dylan; Los Alamos National Laboratory, Earth and Environmental Sciences Kammer, Ryan; Indiana University Bloomington, Indiana Geological and Water Survey

TITLE

Identifying geologic characteristics and operational decisions to meet global carbon sequestration goals

AUTHORS

Richard S. Middleton[1], Jonathan D. Ogland-Hand[2], Bailian Chen[1], Jeffrey M. Bielicki[3], Kevin M. Ellett[4,5], Dylan R. Harp[1], Ryan M. Kammer[4]

[1] Earth and Environmental Sciences, Los Alamos National Laboratory
[2] Department of Earth Sciences, ETH-Zurich
[3] Department of Civil, Environmental and Geodetic Engineering, The Ohio State University
[4] Indiana Geological and Water Survey, Indiana University
[5] Pervasive Technology Institute, Indiana University

ABSTRACT

Geologic carbon sequestration is the process of injecting and storing CO_2 in subsurface reservoirs and is an essential technology for global environmental security (e.g., climate change mitigation) and economic security (e.g., CO_2 tax credits). To meet energy, economic, and environmental goals, society will have to identify vast volumes of high-capacity, low-cost, and viable storage reservoirs for sequestering CO_2. In turn, this requires understanding how major geologic characteristics (such as reservoir depth, thickness, permeability, porosity, and temperature) and design and operational decisions (such as injection well spacing) impact CO_2 injection rates, storage capacity, and economics. Although many numerical simulation tools exist, they cannot repeat the required thousands or millions of simulations to identify ideal reservoir properties and the sensitivity and interaction between geologic parameters and operational decisions. Here, we use *SCO_2T* (pronounced "Scott"; Sequestration of CO_2 Tool)—a fast-running, reduced-order modeling framework—to explore the sensitivity of major geologic parameters and operational decisions to engineering (CO_2 injection rates, plume dimensions, and storage capacities and effectiveness) and costs. Our results show, for the first time, benefits and impacts such as allowing CO_2 plumes to overlap, how different well spacing patterns affect CO_2 sequestration, the effects on costs of including brine treatment and disposal, and the effect of restricting injection rates to 1 $MtCO_2$/yr based on well limitations. We reveal multiple novel and unintuitive findings including: (i) deeper reservoirs have reduced carbon sequestration costs until injection rates reach 1 $MtCO_2$/yr, at which point deeper reservoirs become more expensive, (ii) thicker formations allow for increased injection rates and storage capacity, but thickness barely impacts plume areas, (iii) higher geothermal gradients result in reduced sequestration costs, unless brine treatment/disposal costs are included, at which point reservoirs having lower geothermal gradients are more economical because they produce less water for each unit of injected CO_2, and (iv) allowing plumes to overlap has a significantly positive impact of increasing storage capacities but has only a small influence on reducing sequestration costs. Overall, our results illustrate new scientific conclusions to help identify suitable sites to inject and store CO_2, to help understand the complex interaction between geology and resulting costs, and to help support the pursuit of meeting global sequestration targets.

KEYWORDS

CO_2 capture and storage (CCS); carbon sequestration; *SCO_2T*; reduced-order models; sensitivity analysis.

1.0 INTRODUCTION

Geologic carbon dioxide (CO_2) storage is a component of both CO_2-enhanced oil recovery (CO_2-EOR), where CO_2 is injected into oil fields to increase energy production[1-3], and the CO_2 capture and storage (CCS) process, where CO_2 from large point sources (e.g., coal-fired power plants, iron and steel manufacturing facilities) is captured and compressed, transported in dedicated pipelines, and then sequestered in geologic formations (e.g., deep saline aquifers, depleted shale gas formations)[4-10] (Figure 1). It is also an essential component of negative CO_2 emission technologies such as bioenergy coupled with CCS[11-13] (including biorefineries and biomass power plants) or direct air capture[14-16], which existing climate action plans increasingly rely on to limit warming. Overall, geologic CO_2 storage is a critical technology for environmental, energy, and economic security[17] because it is part of every major climate action plan that limits warming to below 2°C[18-20] and the beneficiary of substantial CO_2 tax credits in the United States (US) that are likely to jumpstart a CO_2 storage industry at a large scale[21-24].

To meet environmental, energy, and economic goals, hundreds of millions or billions of tonnes of CO_2 annually (100s $MtCO_2$/yr to 1+ $GtCO_2$/yr) must be sequestered globally. For example, the Intergovernmental Panel on Climate Change indicates the need to reduce emissions by more than 40 $GtCO_2$/yr by mid-century to achieve net-zero emissions and limit warming to 1.5°C, which some estimate could require up to 300 $GtCO_2$ sequestered by 2050[25]. While studies to date suggest that there is more than enough subsurface storage resource to sequester hundreds of gigatonnes of CO_2—deep saline aquifers are fairly ubiquitous worldwide[26], underlying approximately half of North America, for example[27-29], and resource estimates range between 2,400 and 3,700 $GtCO_2$[30] for the continental United States alone —the storage potential of these geologic formations varies. Meeting the gigatonne challenge requires a significant advance from estimating the prospective geologic storage resource of an area (e.g., US Department of Energy's NATCARB database[28]) to the geologic storage capacity based on explicit consideration of the dynamic processes associated with CO_2 injection and migration. In addition, the geologic properties (e.g., permeability, depth, thickness) have complex and nonlinear interactions that differentially affect the cost of CO_2 storage by factors like the maximum CO_2 injection rate allowed by the formation and the dimensions of the CO_2 plume in the subsurface. As a result, identifying formations and geographic locations to target for geologic CO_2 storage is not trivial and is a pressing challenge. This challenge is only intensified when design and operational decisions, such as allowing CO_2 plumes in the subsurface to overlap (an option for increasing the density of wells at a given CO_2 storage site that may decrease cost) or extracting and treating brine, are also considered. This work aims to contribute to meeting the gigatonne challenge by providing a new and unique capability for evolving from storage resource assessment to the required storage capacity assessment, including cost estimates for CO_2 storage in deep saline formations.

In this study, we perform seven sensitivity experiments that are designed to identify, explore, and quantify CO_2 sequestration properties of geologic formations and to understand why, for example, combinations of geology and operational decisions lead to preferable outcomes such as lower costs, higher injection rates, or higher storage capacities. We evaluate the sensitivity of CO_2 storage performance (rate of CO_2 injection, plume radius, plume volume, storage area density, storage capacity, well density, and cost) to reservoir formation properties (depth, thickness, permeability, porosity, and temperature) and reservoir operational decisions (well spacing, brine extraction and treatment, and realistic injection capacities based on well-casing diameters). The specific operational decisions we consider are (a) constraining CO_2 injection to 1 $MtCO_2$/yr per well, which is a realistic maximum injection rate based on well-casing diameters, (b) the option to allow CO_2 plumes in the subsurface to overlap, and (c) the effect of producing and treating/disposing of subsurface brine, which was previously investigated as a means to minimize induced seismicity and leakage risk and increase CO_2 storage potential[31-33]. This extracted brine must be treated and/or disposed of, with a cost as much as several dollars or more per cubic meter of brine[34]. And, with a representative reservoir CO_2 density of 666 kg/m^3 producing around 1.5 cubic meters of brine for each tonne of CO_2 injected, brine treatment and disposal can add several dollars per tonne to CO_2 sequestration. These operational and design decisions are likely to have substantial ramifications for selecting and prioritizing site selection and, unlike subsurface properties, they are variables that CO_2 storage operators and site planners can control.

The paper is arranged as follows: first, in the background section, we present a literature review of previous sequestration analyses followed by a description of the framework we use, called *SCO₂T*[35], which is designed to perform the sensitivity analyses required for this study. Second, we outline the methodological approach used in our seven sensitivity experiments. Third, we present the results and discussion of the seven analyses. Fourth and finally, we wrap up with conclusions and implications of the research including areas of further exploration and development.

2.0 BACKGROUND

2.1 *Literature review*

Despite the importance of understanding the performance of geologic CO_2 storage to meet global climate goals, the knowledge domain of the CO_2 sequestration science field of study is relatively nascent, in part because appropriately investigating geologic CO_2 storage typically requires using full-physics numerical simulations that are prohibitively resource-intensive. Several sensitivity analysis studies of CO_2 storage performance to uncertain parameters, including storage formation properties and/or operational decisions, have been conducted in recent years using existing tools. Here, we provide an overview of the most relevant studies to the *SCO_2T*-based sensitivity analysis introduced in this paper.

McCoy and Rubin[36] performed a probabilistic analysis that quantified the sensitivity of CCS cost models to variability in design parameters, including pipeline transport model parameters (e.g., pipeline length and inlet/outlet pressure) and geologic parameters (e.g., reservoir permeability, depth, and thickness). Their results showed that the cost of CO_2 injection highly depended on the permeability of the storage reservoir. They also showed that the cost of CO_2 storage increases as reservoir permeability decreases, and the cost of both transport and storage decrease with increasing power plant capacity factor. Stauffer et al.[37] developed a system model called *CO_2-PENS* (Predicting Engineered Natural Systems) for evaluating the viability of CO_2 storage at a range of sites. Monte Carlo simulations can be performed via *CO_2-PENS* to explore complex interactions between uncertain parameters and distinguish the likely performance of potential storage sites. As an example, Stauffer et al.[38] showed how the calculations of the number of wells required and the estimates of plume size can affect long-term storage costs, including decreased costs with increasing reservoir depth. Sifuentes et al.[39] analyzed the impact of various physical properties on the effectiveness of CO_2 sequestration in aquifers. Experimental design-based sensitivity analysis was conducted to identify the most important parameters for the trapping of CO_2. It was observed that horizontal permeability is the most impactful parameter on the total amount of CO_2 dissolved into the brine, and residual gas saturation was found to be the greatest contributor to the total amount of residual CO_2. Also, permeability heterogeneity is a major contributor to both CO_2 trapping mechanisms. Later, Wainwright et al.[40] conducted sensitivity analyses based on a basin-scale reservoir model developed for a hypothetical storage project located in the southern San Joaquin Basin in the US. The impact of uncertainty in parameters (e.g., reservoir permeability, porosity, and pore compressibility) on risk-related performance measures, including the CO_2 plume area and pressure plume size, was evaluated. Three different sensitivity analysis methods—a local sensitivity method, the global Morris method, and the Sobol/Saltelli method—were compared. Results showed that the three analysis methods provided identical interpretations and importance rankings, and that reservoir permeability was identified as the most important parameter for all the performance measures. Metcalfe et al.[41] developed a generic system model using Quintessa's QPAC software, and the model was then applied to the evaluation of CO_2 storage performance at Krechba, near In Salah in central Algeria. Although sensitivity analysis of overall system performance to key operational decisions in the system can be made, the sensitivity analysis of the storage performance including well density and costs to reservoir geologic properties cannot be conducted using their model.

The sensitivity analysis of CO_2 storage performance on uncertain parameters has also been carried out for storage at CO_2-enhanced oil recovery (CO_2-EOR) sites. Dai et al.[42, 43] quantified the sensitivity of a set of risk metrics, including CO_2 injection rate, cumulative CO_2 storage, and the total amount of oil production to uncertain parameters such as reservoir thickness, depth, permeability, and porosity. The results showed that the CO_2 injection rate and the amount of CO_2 storage are most sensitive to reservoir permeability, thickness, and injection pressure. Cumulative oil production is mainly controlled by well spacing, reservoir pay zone, permeability, and initial oil saturation. Chen and Pawar[2] identified key geologic and operational characteristics that affect CO_2 storage capacity and oil recovery potential by performing Monte Carlo simulations and sensitivity analyses. They found that cumulative CO_2 injection is mainly controlled by reservoir permeability and that the total amount of CO_2 retained in the reservoir increases with increased producer bottom-hole pressure, reservoir thickness, and CO_2 injection rate, while it decreases with increased reservoir permeability.

A few system models or tools were developed by researchers to evaluate CO_2 storage performance, but the system models or tools developed in their work cannot perform sensitivity analysis to show how uncertain geologic parameters and/or operational decisions affect the CO_2 storage performance (e.g., injection rate, plume radius, well density, and cost). For example, Zhang et al.[44] developed a system-level model based on *GoldSim* for evaluating CO_2 storage performance in a gas reservoir. However, as mentioned by the authors in their conclusion, the sensitivity analysis of CO_2 storage performance on uncertain geologic/operational parameters could not be performed with their model.

Although previous work examined the sensitivity of carbon sequestration to different geologic parameters and ranges, a comprehensive analysis of how major geologic parameters and operational decisions affect CO_2 storage performance, including both engineering (CO_2 injection rates, plume dimensions, and storage capacities and effectiveness) and costs, has not yet been conducted. This key science gap exists because none of the previously discussed tools, methods, or models can quickly analyze thousands of dynamic reservoir simulations for a single site, or millions over many sites, to identify ideal reservoir properties and the sensitivity and interactions between geologic parameters and operational decisions. Understanding these impacts and complex feedbacks requires a tool that can run while still being able to capture key sequestration processes (i.e., real dynamics of injecting and storing CO_2). That is, the tool should combine the power of full-physics numerical simulations, which are prohibitively resource-intensive, with the speed of systems-level tools (which lack the required physics).

SCO_2T is a systems tool that was originally developed to support sink characterization for the *SimCCS* framework[45, 46], but can be applied to this challenge. Previous *SCO_2T* publications have discussed the *SCO_2T* software and used it to demonstrate well-known sequestration relationships, but did not address these larger knowledge gaps in the sequestration science field[35].

2.2 *SCO_2T*

SCO_2T uses reduced-order models (ROMs) to replicate key outputs from the Finite Element Heat and Mass (FEHM[47-49]) Transfer Code that simulates complex multi-fluid/multi-phase fluid flow (in this case, CO_2 and water). The use of ROMs allows it to maintain nonlinear feedbacks and interactions while being able to simulate thousands of scenarios per second. The tool is able to accurately simulate dynamic CO_2 injection rates and CO_2 plume dimensions (from the full-physics simulator FEHM simulator), using the ROM approach (called Frankenstein's ROMster[50]) and couple outputs with detailed sequestration economics including injection, storage, and brine treatment costs.

It should be emphasized that, even though *SCO_2T* uses perhaps the most detailed economic inputs from the US Environmental Protection Agency (EPA)[51] in a similar approach to the FE/NETL CO_2 Saline Storage Cost Model[52], these costs are still very much uncertain. In reality, they could vary from project to project, one key reason the model includes an uncertainty option. Many costs can also be varied by the user, allowing for uncertainty in storage costs due to project variance to also be addressed. However, even though the impact on costs in our seven experiments is perhaps within the range of uncertainty, it is still illustrative to examine the relative effect on costs. *SCO_2T* assumes the maximum possible injection rate up to 80% of lithostatic pressure. Capturing dynamic plume dimensions is particularly important because it is critical to understanding how efficiently CO_2 can access the pore space and how an operator might spatially arrange injection wells. The model also allows a fractional-well option where a user can allow a non-integer number of wells. This option is useful for sensitivity analysis, where the user doesn't want the model to increase costs in a saw-tooth pattern as new integer wells are added, or to enable direct comparison between different sites particularly with small 2D footprints. See Figure 1 for how plume dimensions can change with, for example, increasing depth.

Although *SCO_2T* has made many advances to enable this current study, particularly capturing dynamic CO_2 injection and storage and linking this to economics, there are many important sequestration aspects that it does not try to simulate (and are not part of this study), many which are available in the models mentioned in the literature review. For example, the model doesn't simulate processes such as wellbore leakage, induced seismicity, or hydrocarbon production. Further, *SCO_2T*, like similar ROM-based approaches, makes key reservoir and modeling assumptions, including lithostatic and hydrostatic pressures, residual water fraction, endpoint relative permeability, more complex geologies, and other parameters including heterogeneity, different fluid properties, and different depositional environments. The current version also does not include monitoring, post-injection, and site closure costs; these will be developed in future versions, along with addressing other model updates, including the ability to simulate injection between 5 and 50 years.

3.0 APPROACH

We use the *SCO_2T* framework to explore how reservoir properties (depth, thickness, permeability, porosity, and temperature) and operational decisions (maximum injection rate, well spacing, and brine treatment) impact the ability to inject and store CO_2 and the final sequestration cost. We analyze how these variables affect CO_2 characteristics that control the injection rate and CO_2 plume dimensions including (i) CO_2 density (kg/m^3) and (ii) CO_2 viscosity (Pa*s). CO_2 density and viscosity principally control how easily CO_2 can be injected and how easily CO_2 can spread out in a reservoir in three dimensions. Consequently, these properties impact key storage parameters including (iii) maximum CO_2 injection rates (MtCO_2/yr), (iv) CO_2 plume radii (km), (v) CO_2 plume volumes (million cubic meters; Mm^3), and (vi) storage area density (MtCO_2/km^2). Storage area density is a measure of storage effectiveness for the 2D footprint of available land and is based on a single non-overlapping CO_2 plume.

We perform a one-at-a-time (OAT) or transect sensitivity analysis across the five key geologic variables[50] to understand the complex interaction of the variables and their impact on sequestration engineering and economics. We also apply a sensitivity analysis to non-geologic and operational variables that have a significant impact on economics including assigning increasing costs to produced brine (brine can be produced to minimize induced seismicity risks and to increase CO_2 storage potential) and allowing CO_2 plumes to overlap by placing CO_2 injection wells increasingly close together.

The paper consists of seven OAT sensitivity analyses that explore the impact on CO_2 injection and storage by varying (1) "artificial" depth through manipulating pressure and temperature independently and jointly, (2) actual depth, (3) reservoir thickness, (4) permeability, (5) porosity, (6) geothermal gradient and brine treatment, and (7) injection-well spacing (overlapping CO_2 plumes). These seven experiments were chosen to cover perhaps the most important range of variable geologic parameters (five) and operational decisions (three); exploration of the geothermal gradients and brine treatment are covered in a single experiment, hence seven experiments. For each experiment, the geologic parameters/ranges and assumptions were chosen to represent realistic parameters from existing studies and field sites while ensuring that critical operational impacts were represented. For example, the impact of limiting injection rates to 1 MtCO_2/yr can only be shown for an experiment with geologic variables, such as permeability, that allow this injection rate. Values for the five key geologic variables are listed in the figures for each experiment.

4.0 Results and Discussion

The color schemes used in charts for each experiment are consistent throughout. For example, from Figure 2, CO_2 density is blue and CO_2 viscosity red throughout all figures in the paper. Charts with dotted lines refer to where the maximum injection rate was limited to 1 MtCO_2/yr. Site- and economic-related outputs, including reservoir storage capacity, number of wells, and final sequestration costs are calculated only using the rate-limited simulations (i.e., when the rate is limited to 1 MtCO_2/yr by the injection well engineering limits); it makes no sense to calculate reservoir economics for a reservoir that could theoretically inject 10 MtCO_2/yr in a single well because typical injection wells will be limited to around 1 MtCO_2/yr. All data for every experiment and figure is available in an Excel Workbook in the supporting information (SI), including the input data to run the *SCO_2T* model and all relevant outputs. The results for the first two experiments—exploring temperature and depth independently and together—are described and discussed in greater detail than the remaining five experiments to avoid repetition in later experiments.

4.1 *Experiment #1: Pressure, Temperature, and Depth*

The first experiment evaluates the impact of formation depth on CO_2 properties and CO_2 sequestration potential. As formation depth can generally be considered positively correlated with pressure and temperature, we use pressure and temperature as a proxy for the formation depth in parts of the analysis. Pressure increases with depth because of the overlying rock and water mass, while temperature increases owing to Earth's geothermal gradient. Figure 2 illustrates the impact of increasing pressure while holding temperature constant (three panels in the top row), increasing temperature while keeping the pressure constant (middle row), and simultaneously increasing pressure and temperature (bottom row). The input data for Figure 2 is provided in the Excel Workbook in the SI.

The formation pressures considered in the top row of Figure 2 range from 9.8 MPa to 29.4 MPa (primary x-axis), which coincides with the formation depth ranging from 1000 to 3000 m (secondary x-axis). Temperature is held at 56°C to isolate the impact of pressure. At 1000 m, 56°C translates into a geothermal gradient of 45°C/km (maximum geothermal gradient plus an 11°C ground surface temperature—this ground surface temperature is used on all simulations in this study) and at 3000 m 56°C translates to a geothermal gradient of 15°C/km (minimum geothermal gradient for *SCO_2T*). The formation temperatures considered in the middle row of Figure 2 correspond to geothermal gradients from 15 to 45°C/km at a depth of 2000 m. This translates into a temperature range of 41 to 101°C. These simulations isolate the impact of temperature on CO_2 properties, injection rates, and plume properties while keeping the pressure constant. The formation depths considered in the bottom row of Figure 2 range from 1000 to 3000 m while letting pressure vary according to the hydrostatic gradient and temperature vary according to a 25°C/km geothermal gradient. (*SCO_2T* also allows users to independently input pressure and temperature based on known values.) The default reservoir hydrostatic pressure is calculated as a function of depth by assuming an average water density of 1000 kg/m^3 with the acceleration of gravity as 9.807 m/s^2. This translates into 9.807 MPa of pressure increase per kilometer of depth.

The pressure and temperature changes associated with increasing depth have opposite impacts on CO_2 properties and sequestration characteristics. Increasing pressure-only (Figure 2abc) increases both the CO_2 density and viscosity (Figure 2a; blue and red lines, respectively). Increased density means that more CO_2 can be stored in the available pore space, increasing the storage area density (Figure 2b; orange line). Increased viscosity typically would lead to a reduced CO_2 injection rate (viscous fluids flow less easily), however, the rate of increase in CO_2 density (which increases injection rates) overpowers the impact of viscosity. Consequently, CO_2 can be injected at a higher rate and thus a greater mass of CO_2 can be injected in a well (Figure 2b; green line). Although increasing CO_2 density means that the plume radius would decrease for a constant injection rate, the increased CO_2 mass (owing to the increased injection rate) overrides this effect and so the plume radius increases with rising pressure (Figure 2c; red line). The same is largely true for plume volume—here, plume volume is the volume of the CO_2 only (equivalent to the injected volume) and not the volume associated with the region of the reservoir where CO_2 can be found in the pore space—where the increasing rate of CO_2 injected overrides the increasing CO_2 density (Figure 2c; purple line). The falling plume volume between 9.8 MPa and 13 MPa is due to the competing effects between CO_2 density and viscosity which both have large rates of change in this range. In *SCO_2T*, the plume volume is only used to estimate the volume of brine that is displaced by the injected CO_2, thus it doesn't consider the rock volume that the plume occupies (i.e., 1:1 relationship between CO_2 plume volume and displaced brine in reservoir conditions). Future versions will potentially generate an actual plume volume ROM.

Increasing temperature-only (Figure 2def) reduces both CO_2 density and viscosity (Figure 2a). Here, the injection rate rises with increasing depth (Figure 2e); the reduced CO_2 density would be expected to reduce the maximum injection rate, but this is overridden by the reduced viscosity of CO_2 and how it influences flow in porous media. Increasing temperature has a more complex impact on the storage area density (Figure 2e). Up to 66°C the storage area density is relatively constant at around 0.4 $MtCO_2/km^2$ (66°C corresponds to a geothermal gradient of 27.5°C/km and 11°C for the ground surface temperature) because the impacts of CO_2 density and the larger mass of CO_2 injected balance each other. Beyond 66°C, the storage area density falls because the injection rate does not continue to rise quickly enough to counterbalance the reduced CO_2 density. The plume radius and plume volume both rise with increasing temperature (Figure 2f); increased injection rates and reduced CO_2 density increase both the volume of the plume and how far the plume spreads. The CO_2 injection rate never reaches the 1 $MtCO_2$/yr maximum.

Figure 2ghi illustrates the impacts when pressure and temperature are both allowed to increase simultaneously as depth goes from 1000 to 3000m. Pressure (Figure 2a) and temperature (Figure 2d) have opposing impacts on CO_2 density and viscosity, which are nearly balanced out when pressure and temperature vary naturally with depth (Figure 2g). However, the overriding impact of CO_2 density means that both the injection rate and storage area density both rise with increasing depth (Figure 2h); in this case, the impact of pressure has a much greater impact than temperature. In the case of the plume radius and volume, increasing depth forces both to rise (Figure 2i). Interestingly, despite their counterbalancing effects, the combined impacts of pressure and temperature lead to both higher (in deeper formations) and lower (in shallower formations) values for CO_2 injection rates and storage area capacities (Figure 2h) and plume radii and volumes (Figure 2i) than that for pressure (Figure 2bc) and temperature (Figure 2ef) independently.

This first experiment illustrates that there is a complex and nonlinear interaction between pressure and temperature in terms of CO_2 properties and sequestration characteristics. Being able to capture these effects is critical for understanding sequestration, particularly when coupled with economics. This further demonstrates the need for reduced-order modeling approaches to be able to capture effects that are typically captured only when using full-physics numerical models but with the speed of analytical models.

4.2 *Experiment #2: Depth*

The second experiment is a more traditional exploration of the impacts of increasing depth on sequestration engineering and economics, where formation depth is increased from 1000 to 5000 m while holding the remaining four geologic variables constant (Figure 3). The solid lines in Figure 3a and Figure 3b represent simulations where the injection rate is unlimited, whereas the dotted lines represent simulations where the injection rate is limited to the 1 $MtCO_2$/yr maximum rate governed by well-casing diameters. For the unlimited runs, the injection rate and plume radius both rise with increasing depth, though the rate of increase in the plume radius slowly declines (Figure 3a). Consequently, the plume volume and storage area density for the unlimited simulations also rise with increasing depth (Figure 3b). Although the plume area radius increases, the storage density increases faster than the expanding plume radius (the CO_2 plume expands at the bottom of the formation faster than the spread at the top of the formation; see the Thickness Experiment below for more details). In this experiment, the rate of increase in CO_2 density caused by the pressure increase overrides the decrease in CO_2 density by temperature. Consequently, more CO_2 can be injected with depth and more effectively or more densely occupies the available pore volume given the parameters in this experiment.

Limiting the injection rate to 1 $MtCO_2$/yr imparts significant changes (Figure 3a and Figure 3b). The 1 $MtCO_2$/yr injection rate is reached at a depth of 2850 m (see data in the SI for Figure 3). At this threshold, the simulated injection rate is capped at exactly 1 $MtCO_2$/yr (Figure 3a; green dotted line). However, the rate-limited plume area linearly declines after the 2850 m depth is reached (Figure 3a; red dotted line). That is, if you inject a constant amount of CO_2, the distance the CO_2 migrates laterally decreases as the formation depth increases because that same amount of CO_2 occupies a smaller 3D space (i.e., is denser). Put another way, the plume area in the unlimited case continues to expand because the increasing rate of CO_2 injected overrides the impact of more-densely stored CO_2. In our case, the CO_2 plume volume—the volume of the injected CO_2—remains relatively steady (but not flat) after 2850 m because the competing effects of pressure and temperature keep the CO_2 density relatively flat (Figure 3b; dotted purple line). After the 1 $MtCO_2$/yr threshold is reached, the storage area density continues to rise but not quickly as in the unlimited case (Figure 3b; orange dotted line). This is because the plume radius falls in the rate-limited case and thus, in terms of 2D storage area density, the storage effectiveness still increases even though the injection rate is held at 1 $MtCO_2$/yr.

The bottom panes in Figure 3 (Figure 3c and Figure 3d) illustrate the logistic and economic sequestration impacts. The bottom two panels in Figure 3, Figure 4, Figure 6, and Figure 7 are all based on rate-limited simulation results. Storage capacity rises with increasing depth (Figure 3c; olive-colored line); all simulations assume a 256 km^2 (16 x 16 km) surface footprint for a reservoir. The storage capacity of the reservoir is closely related to the storage area density. The storage area density is based on a single CO_2 plume within a fixed area, while the reservoir storage capacity is based on injecting CO_2 into multiple wells within a fixed area considering the space between plumes and areas of plume overlap. The number of wells that can be placed in the 16 x 16 km area decreases as thickness increases (because the CO_2 plume 2D footprints get larger and larger) until the point when the injection rate reaches the 1 $MtCO_2$/yr threshold (Figure 3c; light blue line). The number of wells is calculated by working out how many injection plumes could be placed in the available area, accounting for the spatial arrangement of wells and the amount of allowable overlap. In all cases apart from the Well Spatial Arrangement Experiment, all wells are assumed to be placed in a hexagonal pattern with no plume overlap. Further, to ensure that the sensitivity analysis is not affected by the integer nature of wells, we use the *SCO_2T* fractional well option. Once the 1 $MtCO_2$/yr threshold is reached, the plume radius falls and the number of wells that can be placed in the available area rises. The number of wells that are required to maximize the injection rate in the 16 x 16 km area and the injection rate of each well are the two key parameters for calculating overall sequestration costs (Figure 3d; teal line). *SCO_2T* has customizable options that exogenously impact costs: whether to include costs to pump CO_2 (no pumping is required if CO_2 arrives at the wellhead at suitable pressure), cost to drill brine production wells, and cost to treat brine. Here, in all cases apart from the Geothermal Gradient and Brine Treatment Experiments, these costs are set to zero. Down to the 2850 m (or 1 $MtCO_2$/yr) threshold, sequestration costs decline because fewer wells are required *and* more CO_2 can be injected in each well (site-wide fixed costs, such as 3D seismic surveys and site preparation, are constant). However, beyond the threshold, the costs rise because, even though storage area density still increases, the storage effectiveness of each well declines.

This last point is critical for understanding the suitability of sequestration characteristics; looking at injection rates or storage area density or storage capacity alone is not a good indicator of sequestration suitability. Here, imagine comparing two hypothetical reservoirs where all formation properties are identical except that one has a depth of 3000 m and the other 5000 m. The latter has a higher injection rate, higher storage area density, and a higher total reservoir capacity, yet its costs are more than 10% higher (\$4.35/tCO_2 versus \$3.92/tCO_2). This is a key attribute of *SCO_2T* and how the framework captures the complexity and fidelity of sequestration engineering (e.g., limited and unlimited injection rates, plume dimensions) and links it to sequestration economics based on the actual logistics of injecting and storing CO_2.

4.3 *Experiment #3: Thickness*

The third experiment examines the impact of increasing formation thickness (Figure 4). As thickness increases from 5 to 100 m, the unlimited CO_2 injection rate, in this case, climbs from 0.14 $MtCO_2$/yr to almost 2 $MtCO_2$/yr (Figure 4a). The unlimited CO_2 injection rate, again, is simply the case where the injection rate is not limited to the maximum 1 $MtCO_2$/yr rate enforced by the well engineering limits. This is an almost 15-fold increase in the injection rate as the thickness increases by 20 times. At the same time, the CO_2 plume radius is almost flat, with only a slight decrease. That is, even though the CO_2 injection rate increases by 15 times, the plume radius is almost unchanged. Although the theoretical shape of CO_2 plumes was investigated previously (e.g., Nordbotten et al.[53]), this effect was unexpected and has perhaps not been clearly documented in the literature. Here, although the mass (and volume) of CO_2 massively increases, the available pore space increases at a faster rate and the plume does not have to spread out as far. Figure 5 illustrates this unexpected result through a series of full-physics FEHM-simulated CO_2 plumes in formations with varying formation thickness that correspond to the simulations in Figure 4. When the injection rate is limited to 1 $MtCO_2$/yr (occurring at a thickness of 46 m) the CO_2 plume radius reduces with increasing thickness (Figure 4a; dotted red line) because the injected CO_2 mass is constant, whereas the available pore volume continues to increase. *SCO_2T* assumes that the screen size—the vertical extent of the wellbore where CO_2 can pass into the formation—stretches across the entire formation thickness. The CO_2 plume volume expands correspondingly with the limited and unlimited injected CO_2 mass (no changes in CO_2 density and temperature), while the storage area density rises with increased thickness (Figure 4b). However, the storage area density for the limited injection rate is not quite as high as for the unlimited injection rate (i.e., where the injection rate can be greater than 1 $MtCO_2$/yr), indicating that the effect of increased thickness outweighs the effect of the decreased CO_2 plume radius.

The reservoir storage capacity increases correspondingly with the rising storage area density (Figure 4c). The number of wells corresponds with the plume radius based on the limited injection rate; once the 1 $MtCO_2$/yr kicks in at 46 m, the number of wells increases because the footprint of the plumes is smaller and thus more wells can be packed together. The rapidly increasing injection rate and storage area density coupled with the constant number of wells (up to a thickness of 45 m) means that the sequestration cost drops by more than 50%—\$11.19/tCO_2 to \$4.93/tCO_2 from 5 to 45 m (Figure 4d). Beyond a thickness of 45 m, the sequestration costs are flat because the increased cost of using more wells is balanced out by the increased storage area density.

4.4 *Experiment #4: Permeability*

The fourth experiment focuses on the impact of increasing permeability (Figure 6). Permeability is well-known to affect injection rates which, in turn, has a significant impact on sequestration costs. Figure 6a shows injection rates rapidly increasing as permeability rises from 1 to 150 mD, which in turn increases the CO_2 plume radius (Figure 6a). When the injection rate is capped at 1 $MtCO_2$/yr (at 82 mD in the experiment), the CO_2 plume radius continues to expand (though less quickly than the unlimited injection case) because the increased permeability allows the CO_2 to migrate laterally more easily. The rate of increase of the CO_2 plume radius gradually declines between 1 and 60 mD before reaching a near-steady rate of increase (Figure 6a). The CO_2 plume volume (i.e., the volume of brine that is displaced by the injected CO_2) is directly related to the unlimited/limited CO_2 injection rate (compare the green line in Figure 6a with the purple line in Figure 6b). The storage area density increases between 1 and 60 mD (Figure 6b), corresponding to the part of the CO_2

plume radius that has a decreasing rate of increase (Figure 6a). Beyond 60mD, the storage area density is flat for the unlimited injection rate because the effect of injected CO_2 mass and plume radius on storage area density cancel each other out. In the limited injection case (i.e., beyond 82 mD) the storage area density declines because the injection rate is constant but the CO_2 plume radius continues to increase.

Because the plume radius continues to expand for the limited injection rate (and unlimited also), the number of wells decreases as permeability rises from 1 to 150 mD (Figure 6c). The reservoir storage capacity follows the same general trend as the storage area density: the capacity rises between 1 and 60 mD, is flat until the 1 $MtCO_2$/yr threshold is reached (at 82 mD), and then the reservoir storage capacity falls (even though each well has the same injection rate, their plume radii are larger). These effects combine for a nonlinear impact on sequestration costs (Figure 6d). Sequestration costs drop exponentially from around \$40/tCO_2 at 1 mD (injection rate of 0.015 $MtCO_2$/yr) to around \$6.50/tCO_2 once permeability rises to 20 mD (injection rate of 0.25 $MtCO_2$/yr). This exponential decline in costs as injection rates rise to around 0.25 $MtCO_2$/yr has been shown previously[54]. Subsequently, sequestration costs keep falling to \$4.64/tCO_2 at a permeability of 82 mD before slowly rising to \$4.92 at 150 mD. The steady increase in costs after 82 mD is caused by the decline in storage area density (i.e., storage effectiveness).

4.5 *Experiment #5: Porosity*

The fifth experiment focuses on porosity (Figure 7) and is the simplest in the sense that porosity does not affect CO_2 density, CO_2 viscosity, or the movement of CO_2. Consequently, the CO_2 injection rate is flat as porosity moves from 0.05 to 0.4 (Figure 7a). Although porosity does not affect the movement of CO_2 in our experiment, the plume radius does decline because a greater volume of pore space can be filled in all directions. A linear change in porosity does not have a linear effect (decline) on the plume radius because the 2D radius is a function of the 3D plume shape or volume. Because the injection rate does not change, the CO_2 plume volume does not change while the storage area density increases along with the linear increase in pore volume (Figure 7b). Consequently, both the reservoir storage capacity and the number of wells increases nearly linearly with porosity (Figure 7c). At first, it seems intuitive that reservoirs having higher porosities would require more wells, but it becomes evident when considering that the plume radii do decrease with increasing porosity. Although the number of wells rises, the effect of the linear increase in storage area density overcomes the effect of the increase in the number of wells on total sequestration cost, which declines with increased porosity (Figure 7d).

4.6 *Experiment #6: Geothermal Gradient and Brine Treatment*

The sixth experiment explores the effect of geothermal gradient with and without the costs of treating produced brine (Figure 8). Note that, although the effect of an increasing geothermal gradient on CO_2 injection, plume dimensions, and storage area density has already been described in the first experiment (Figure 2d, Figure 2e, and Figure 2f), the bounding geologic parameters are slightly different in experiment #6. As noted previously, extracting brine is likely to be critical for large-scale sequestration as a means to minimize induced seismicity, minimize CO_2 leakage risk, and increase CO_2 storage potential, and that treating and disposing of this brine will lead to additional sequestration costs. In *SCO_2T*, the user inputs their desired \$/m^3 cost to treat and dispose of brine.

In this experiment, the geothermal gradient increases from 15°C/km to 45°C/km—formation temperature rises from 41°C to 101°C using a constant depth of 2000 m—the CO_2 injection rate rises in linear steps or pieces and the plume radius rises almost linearly (Figure 8a). The rising injection rate and falling CO_2 density lead to a rapidly increasing plume volume (Figure 8b). Because the injection rate increases fastest up to 60°C, the storage area density happens to rise with increasing temperature (Figure 8b). Once the rate of increase in the injection rate reduces slightly, between 60°C and 78°C, the storage area density declines slowly (i.e., a tipping point). Then once the rate of increase in the injection rates falls more steeply (after 78°C), the storage area density notably declines. However, it should be noted that the storage area density varies only between around 0.27 $MtCO_2/km^2$ and 0.29 $MtCO_2/km^2$ as the geothermal gradient is changed from 15°C/km to 45°C/km because the injection rate and plume radius increase very similarly.

The number of wells falls almost linearly (Figure 8c) as a result of the increasing plume radius, dropping from 4.5 wells to 2.8 wells. The reservoir storage capacity (Figure 8c) follows the same pattern as the storage area density plot, with the total available capacity varying no more than a few percent as the geothermal gradient increases from 15°C/km to 45°C/km. That is, even though the number of wells that can be placed within the 2D area falls, the increased injection rate for each well compensates and so storage capacity is not significantly affected. The final result for the simulations with no brine treatment costs (bottom curve in Figure 8d) is that sequestration costs fall with the increasing geothermal gradient; total sequestration costs fall from \$3.55/tCO_2 (15°C/km) to \$3.07/tCO_2 (45°C/km). The CO_2 density drops from 829 kg/m^3 (geothermal gradient of 15°C/km) to 466 kg/m3 (45°C/km), illustrating that more brine is produced as the geothermal gradient increases (CO_2 density is not shown in the chart). *SCO_2T* assumes that the CO_2 displaces an equal volume of brine. That is, even though the plume area expands (ultimately reducing storage area density), each well can inject more CO_2 with the increasing geothermal gradient, and costs ultimately fall. However, assigning a cost to treating brine changes this relationship, where, ultimately, higher geothermal gradients result in increased costs (top two lines in Figure 8). That is, the cost to treat the increased brine production outweighs the savings from injecting more CO_2. For example, a brine treatment cost of \$1/m^3 of brine (middle lines in Figure 8) sees costs fall slightly between 41°C to 61°C (\$4.74/tCO_2 to \$4.64/tCO_2) before rising to \$5.14/tCO_2. With \$2/m^3 brine treatment cost, sequestration costs rise almost continuously from \$5.96/tCO_2 to \$7.21/tCO_2. Consequently, sequestration costs having a \$2/m^3 brine treatment cost are between 1.68 times (15°C/km) to 2.35 times (45°C/km) higher than if brine is not produced or treated. A more than doubling of sequestration costs could have a significant impact on sequestration economic analysis.

4.7 *Experiment #7: Well Spatial Arrangement*

Experiment #7 explores the impacts of arranging the injection wells in different patterns, focusing on the effect of allowing plumes to overlap. At the outer edges of the plume, the CO_2 density is very low, and so plume interaction is relatively minor with relatively low or no negative impacts. Figure 9 illustrates the concept of overlapping plumes and how the same number of plumes (nine in this visualization) can be fit into a smaller area when plume overlap is allowed. Consequently, the storage area density is increased as the pore space is used more effectively. This experiment uses the overlapping plume capability to explore the effect of allowing plumes to overlap between 0% and 50% (Figure 10). Note, the tool is a sequestration screening or feasibility tool based on individual injection wells and does not attempt to capture the pressure interaction between multiple plumes; instead, it assumes that pressures are managed through brine extraction. For an experiment with a 50% overlap, this means that 50% of the area (not radius) of a plume is overlapped by surrounding plumes, where the outer parts of the plume's horizontal extent have a lower storage area density (i.e., thinner layer of CO_2) than closer to the center of the plume. Here, varying the plume overlap between 0 and 50% increases the storage capacity from 58 $MtCO_2$ to 97 $MtCO_2$ (Figure 10a; olive line), an increase of

67%, while the storage area density rises from 0.29 $MtCO_2/km^2$ to 0.39 $MtCO_2/km^2$ (orange line in Figure 10a) an increase of 35%. Allowing plumes to overlap means that more wells can be placed in the same 2D area. Consequently, the number of wells rises from 3.4 to 5.7 (Figure 10b; light blue line), a rise of 28%. Although having more wells translates into greater fixed capital and fixed O&M costs, more CO_2 can be stored in the same 2D footprint and so overall sequestration costs fall from \$6.13/tCO_2 to \$5.75/tCO_2 (Figure 10b; dark blue line). However, this represents only a 6% drop in costs, which is essentially a function of the fixed site-wide costs (e.g., purchasing land/pore space, permitting, seismic imaging) being spread over a greater amount of stored CO_2. That is, costs directly related to drilling and operating each well do not change by letting plumes overlap. A way to visualize this is to examine the 2D cross-profiles of potential plumes in Figure 5; even with a high allowable overlap, the parts of the plume with a high storage density never overlap.

5.0 Conclusions and Implications

Meeting global climate challenges will require identifying CO_2 sequestration sites on the scale of hundreds of billions of tonnes of CO_2, which is orders of magnitude larger than current CO_2 sequestration levels. For example, worldwide CO_2-enhanced oil recovery infrastructure currently sequesters less than 100 $MtCO_2$/yr, and anthropogenic storage of CO_2 is around 40 $MtCO_2$/yr[55]. In an effort to investigate the impact that subsurface parameters and operational decisions have on the suitability of geologic CO_2 storage at this scale, this study performed a set of sensitivity analyses using *SCO_2T*. The tool was used because it was designed to be able to quickly capture complex and nonlinear interactions between geologic parameters—formation depth, thickness, permeability, porosity, and temperature—and properties such as density and viscosity, and how this affects CO_2 injection rates, plume dimensions, storage capacity, and overall economics. As such, the primary finding of this study is the demonstration that it is possible to perform this required sensitivity analysis to understand sequestration, which was up to now was a daunting and perhaps prohibitive task to undertake using full-physics numerical models.

Our results and discussion are intended to help guide the emerging challenge of identifying suitable storage sites on a massive scale. Our new findings are grouped into four sets of unexpected or previously unknown conclusions:

1. *Limiting injection rates to a realistic 1* $MtCO_2$*/yr per injection well has substantial impacts on sequestration engineering and economics, even to the degree that presumed ideal geologic conditions could become less favorable.* For example, results show that while identifying reservoirs with larger thicknesses (Experiment #3; Figure 4) and higher porosity (Experiment #5; Figure 7) is typically going to result in improved sequestration, deeper reservoirs (Experiment #2) and higher permeability reservoirs (Experiment #4; Figure 6) can have poorer sequestration performance once the 1 $MtCO_2$/yr rate is reached. In the case of permeability, this effect is relatively minimal, but is significant for depth: this suggests that using deeper reservoirs reduces carbon sequestration costs until injection rates reach 1 $MtCO_2$/yr (engineering-limited rate of injection), at which point deeper reservoirs cost more. This rate-limiting theme has the potential to have a significant impact on how we reach aggressive sequestration targets.

2. *Thicker formations allow for larger injection rates and storage capacity but not plume area.* The impact of thickness on sequestration and economics was partially unexpected and potentially significant for large-scale CO_2 injection and storage. Our results show that the radius of the CO_2 plume remains relatively constant—which was unexpected and not previously documented—and may even decrease, with increasing reservoir thickness. This occurs even though increasing thickness also increases the CO_2 injection rate as

well as the total CO_2 storage capacity (Experiment #3; Figure 4). This unexpected relationship is itself a finding that deserves to be more clearly documented in the geologic CO_2 storage literature, but it may also have large ramifications on what geologic formations are targeted for CO_2 storage because monitoring costs are largely a function of plume size.

3. *Sites having higher geothermal gradients could have reduced sequestration costs unless brine treatment/disposal costs are included, at which point sites with lower geothermal gradients may cost less.* The geothermal gradient also has unexpected impacts on CO_2 injection and storage rates and costs. Our results show that an increasing geothermal gradient generally reduces CO_2 storage costs because the well injection rate increases faster than the reduction of stored CO_2 (owing to reduced density of CO_2). This would suggest, all things being equal, that geologic formations having higher geothermal temperature gradients should be targeted for geologic CO_2 storage before those with lower geothermal temperature gradients. However, this relationship inverts when including the cost to extract and treat brine (Experiment #6; Figure 8). Extracting brine might be needed to minimize induced seismicity risks while increasing the CO_2 storage potential by freeing-up pore space. Treating brine not only adds an additional cost regardless of the geothermal gradient, costs rise with an increasing gradient (as opposed to falling without brine treatment) because each tonne of stored CO_2 displaces an increasingly larger volume of brine. This could have substantial implications for choosing geologic reservoirs for CO_2 storage. Future studies could consider treating the brine—particularly hot mineral-laden brines— as a resource that could help mitigate the cost of CCS instead of adding to it. For example, it could be possible to chain sequestration, geothermal energy (electricity or direct heat), mineral extraction, and water treatment technologies together to produce an integrated system that uses the economic value of the brine (heat, minerals, and freshwater) to offset sequestration costs or to increase system profitability.

4. *Allowing plumes to overlap has a significantly positive impact on increasing storage capacities but only a small impact on reducing sequestration costs.* In other words, motivation for designing CO_2 storage sites with overlapping CO_2 plumes should be driven by the need to increase the amount of CO_2 stored at the site, and less by the need to reduce the \$/tCO_2 cost. To our knowledge, this is the first study to investigate the effect of letting CO_2 plumes overlap and the subsequent impact on storage rates and economics. Our results suggest that the marginal increase in CO_2 storage capacity resulting from allowing CO_2 plumes to overlap by 50% may be an order of magnitude larger than the resulting marginal decrease in cost, in part, because the costs related to drilling and operation of the wells do not change if plumes overlap (Experiment #7; Figure 10). That is, there is only a moderate reduction in cost by packing wells closer together even though there is a significant increase in storage capacity. However, there could be other significant drivers to place wells closer together such as more efficiently using the land surface to minimize environmental impacts or to deal with fewer landowners or pore space owners. Further, the *SCO₂T* tool is a screening or feasibility tool and does not take into account the pressure interaction between plumes and instead assumes that pressure is being managed through brine extraction.

Overall, the seven experiments illustrate that there are complex interactions between geologic variables and sequestration engineering and economics, and that this will almost certainly have a significant impact on society reaching global sequestration goals. The experiments indicate that design and operational decisions—maximum injection rates, brine treatment, and overlapping CO_2 plumes—can have a significant impact on the feasibility of site-scale geologic sequestration and should be considered in future studies. Also, the results show that, when trying to assess the suitability of potential sequestration sites, it is important to explore the range of simulation outputs and not just to look at injection rates or storage area density or storage capacity alone.

6.0 ACKNOWLEDGMENTS

This research was primarily funded by the US Department of Energy's (DOE) Fossil Energy Office project "*SimCCS*: Development and Applications" (Award No. FE-1017-18-FY18). Additional work was funded by DOE's Fossil Energy Office through the "Carbon Utilization and Storage Partnership (CUSP) for the Western USA" (Award No. DE-FE0031837) and the "Southeast Regional CO_2 Utilization and Storage Acceleration Partnership (SECARB-USA)" (Award No. DE-FE-0031830), the "US-China Advanced Coal Technology Consortium" (Award No. DE-PI0000017), and through Los Alamos National Laboratory's Laboratory Directed Research Development program (LDRD; Award No. 20190057DR).

585 # 7.0 FIGURES

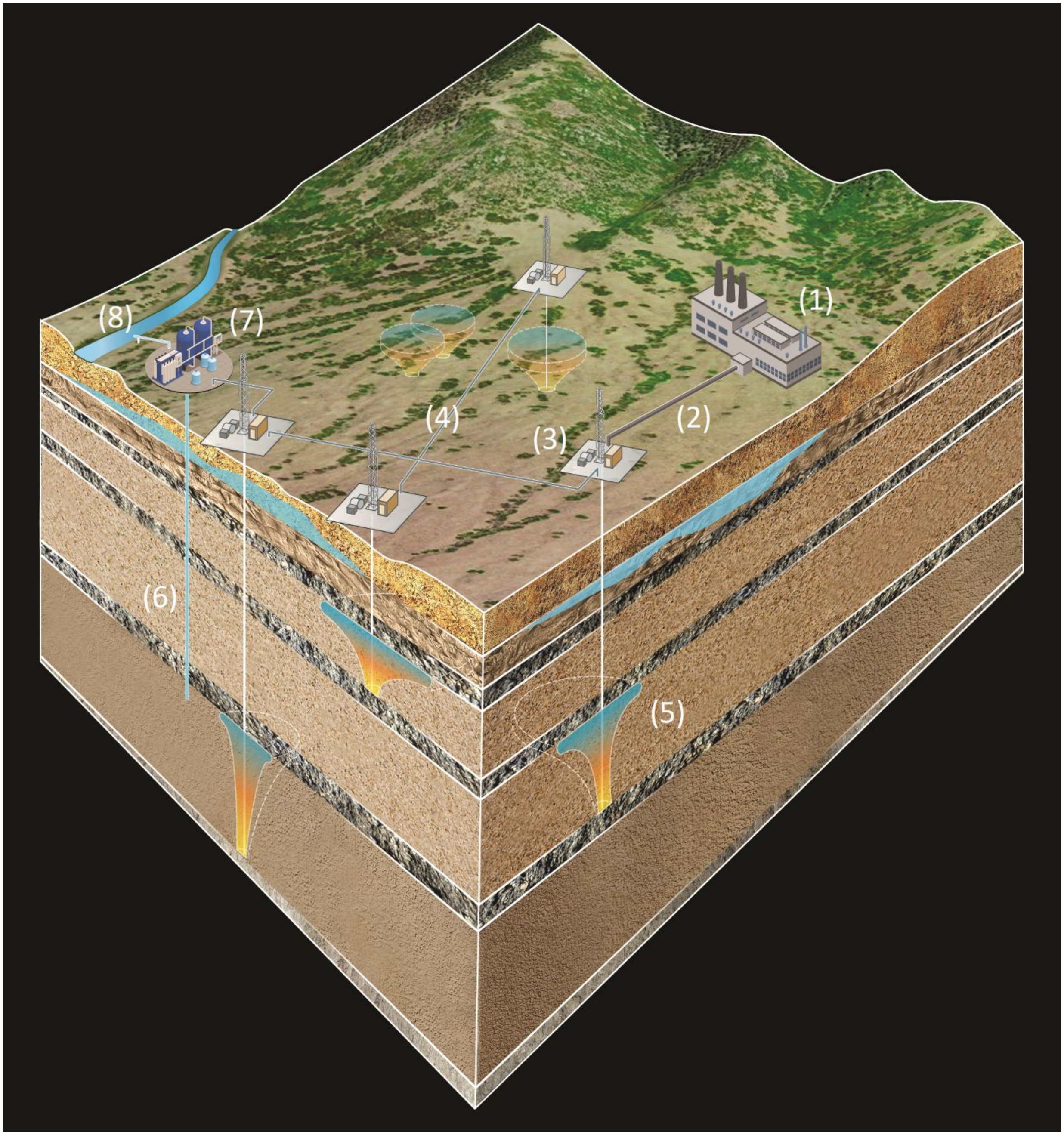

Figure 1: Overview of site-scale sequestration including (1) CO_2 sources such as a coal-fired power plant, (2) CO_2 pipeline network delivering CO_2 to the sequestration complex, (3) CO_2 injection well, (4) site-scale pipeline network distributing CO_2 between injection wells, (5) CO_2 plumes, (6) brine extraction, (7) brine treatment facility, and (8) end-use for treated water including disposal into surface water systems. The grey layers indicate caprock layers through which CO_2 cannot migrate, while the brown layers are indicative of CO_2 being stored in sandstone formations. The CO_2 plumes are colored for visual purposes only.

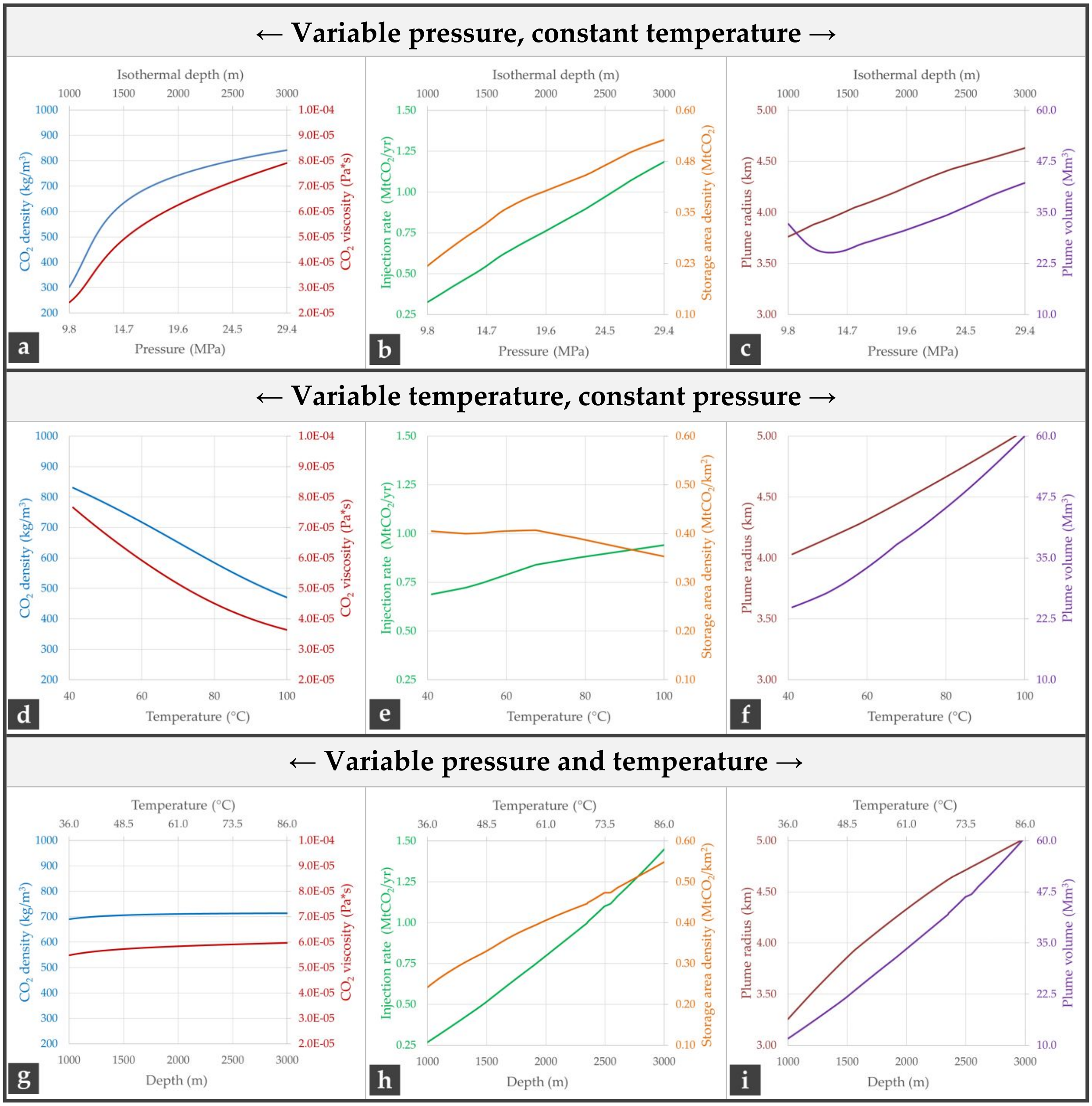

Figure 2: Impact of pressure-only (constant temperature; top row), temperature-only (constant pressure; middle row), and depth (pressure and temperature varying with depth; bottom row) on CO_2 density and viscosity (a, d, g), injection rate and storage area density (b, e, h), and plume radius and volume (c, f, i). Temperature is held constant at 66°C (associated with a formation depth of 2000 m) for the constant pressure runs. The y-axes in each chart have the same minimum and maximum values, whereas the x-axis always corresponds to pressure and temperature changes as depth increases from 1000 to 3000 m.

586

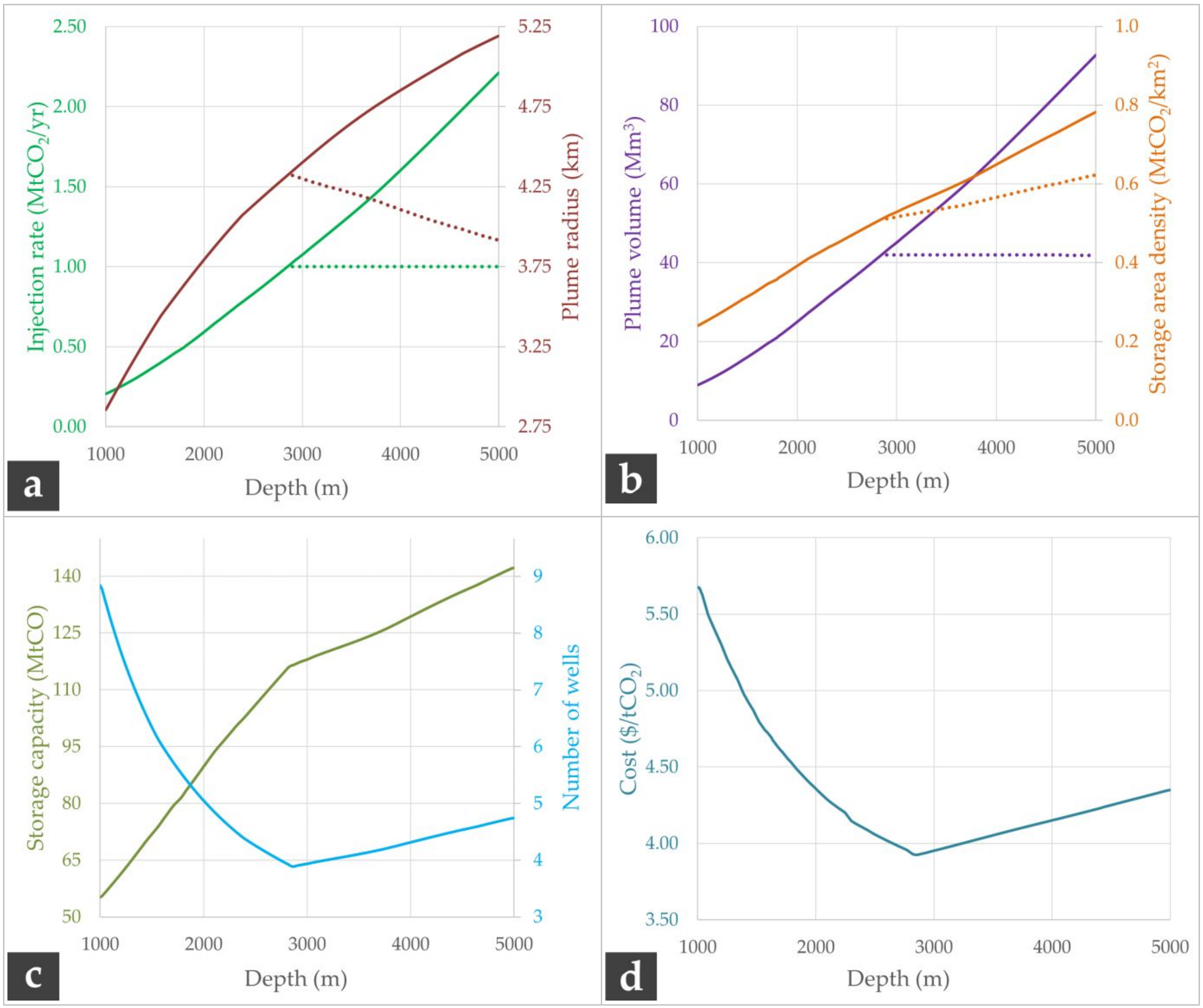

Figure 3: Impact of depth on: (a) injection rate and plume radius; (b) plume volume and storage area density; (c) reservoir storage capacity and number of wells used; and (d) CO_2 injection/storage costs. Depth ranges between 1000 and 5000 m while thickness (10 m), permeability (15 mD), porosity (0.2), and geothermal gradient (25°C/km) are held constant. Dotted lines indicate that the injection rate was capped at 1 $MtCO_2$/yr, illustrating divergences from the uncapped simulations (solid lines).

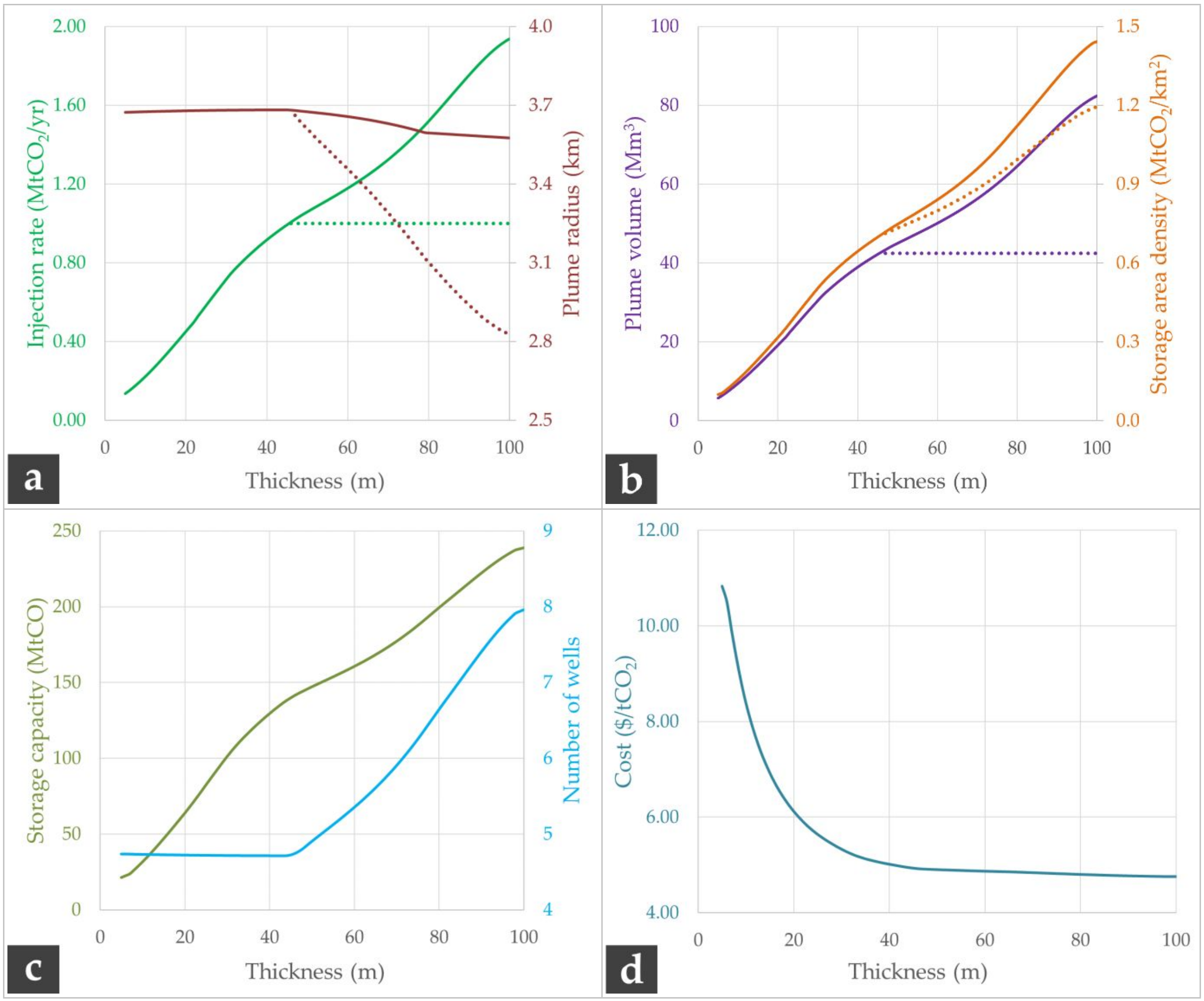

Figure 4: Impact of formation thickness on: (a) injection rate and plume radius; (b) plume volume and storage area density; (c) reservoir storage capacity and number of wells used; and (d) CO_2 injection/storage costs. Thickness ranges between 5 and 100 m, while depth (1500 m), permeability (18 mD), porosity (0.2), and geothermal gradient (25°C/km) are held constant.

588

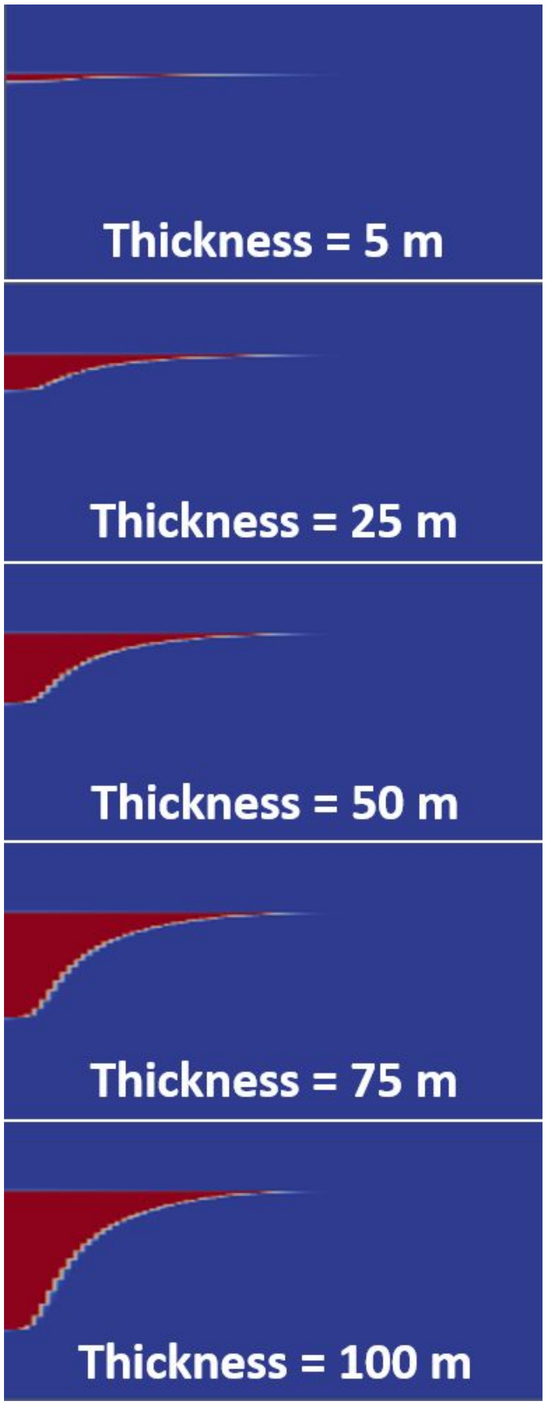

Figure 5: Impact of formation thickness on plume dimensions; full physics FEHM simulations for the reduced-order *SCO₂T* results in Figure 4. The vertical axis is exaggerated by five times. Red indicates the CO_2 plume.

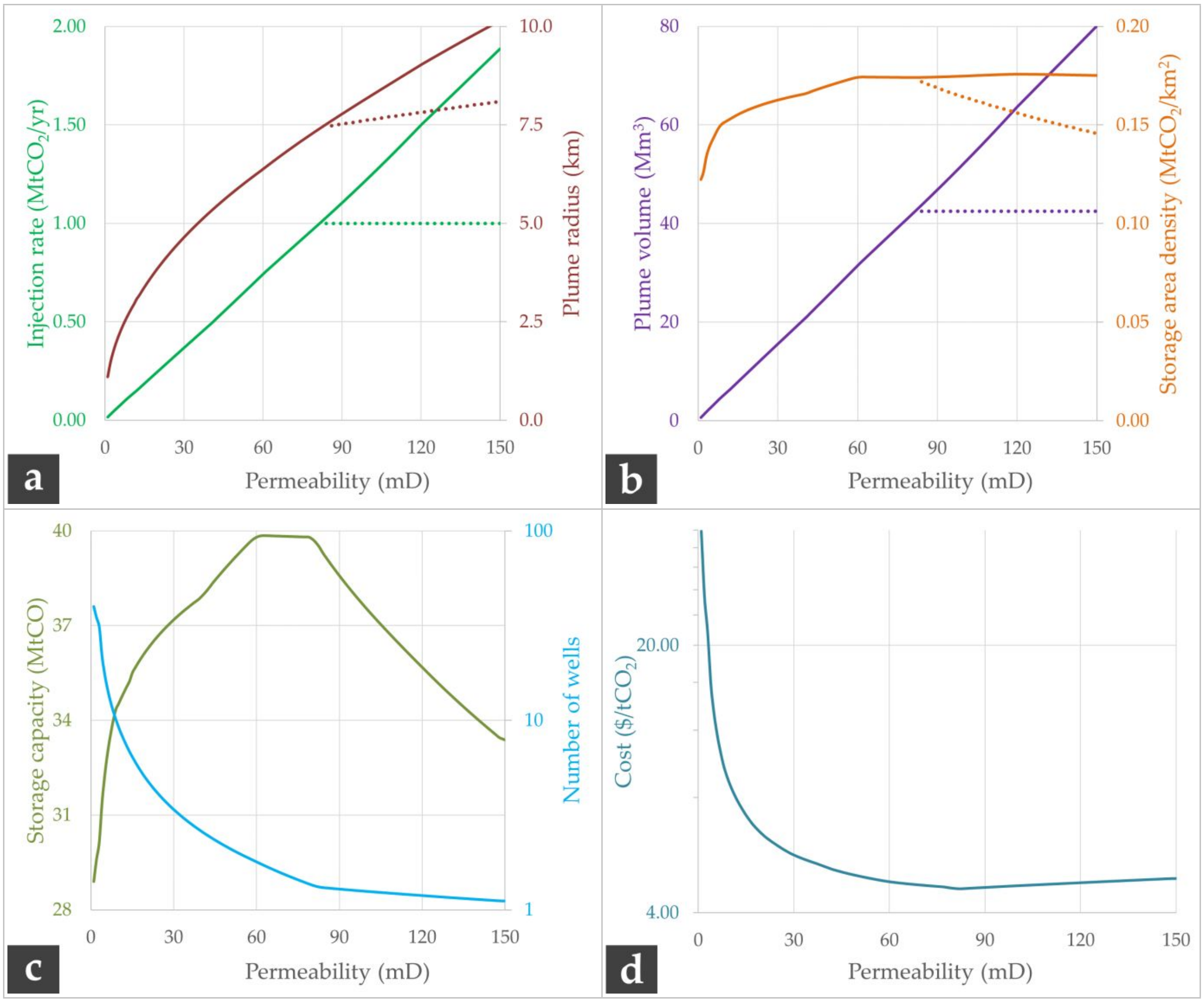

Figure 6: Impact of permeability on: (a) injection rate and plume radius; (b) plume volume and storage area density; (c) reservoir storage capacity and number of wells used; and (d) CO_2 injection/storage costs. Permeability ranges between 1 and 150 mD while depth (1500 m), thickness (10 m), porosity (0.2), and geothermal gradient (25°C/km) are held constant. Dotted lines indicate that the injection rate was capped at 1 $MtCO_2$/yr illustrating divergences from the uncapped simulations (solid lines).

589

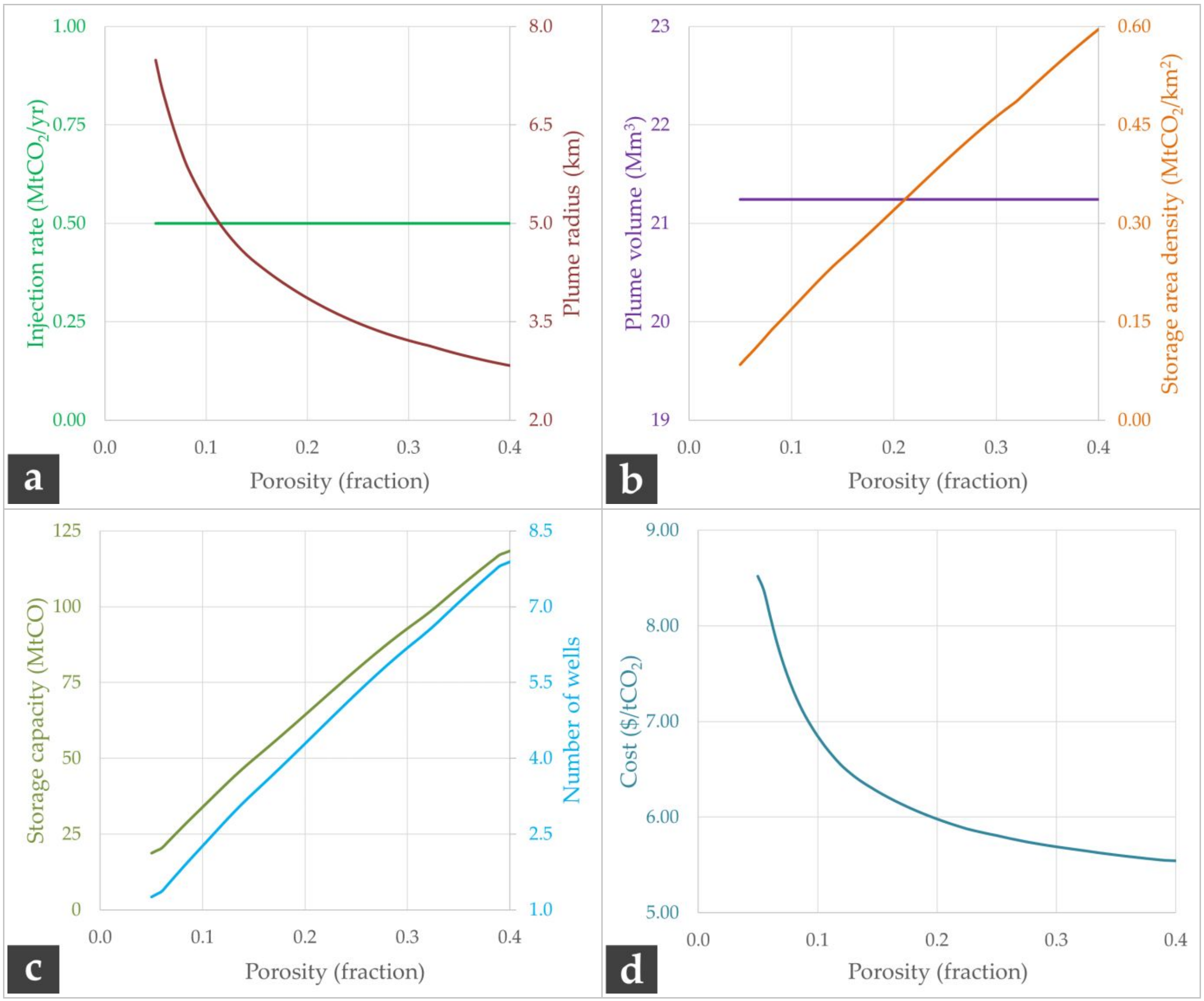

Figure 7: Impact of porosity on: (a) injection rate and plume radius; (b) plume volume and storage area density; (c) reservoir storage capacity and number of wells used; and (d) CO_2 injection/storage costs. Porosity ranges between 0.05 and 0.4 while depth (1500 m), thickness (10 m), permeability (20 mD), and geothermal gradient (25°C/km) are held constant.

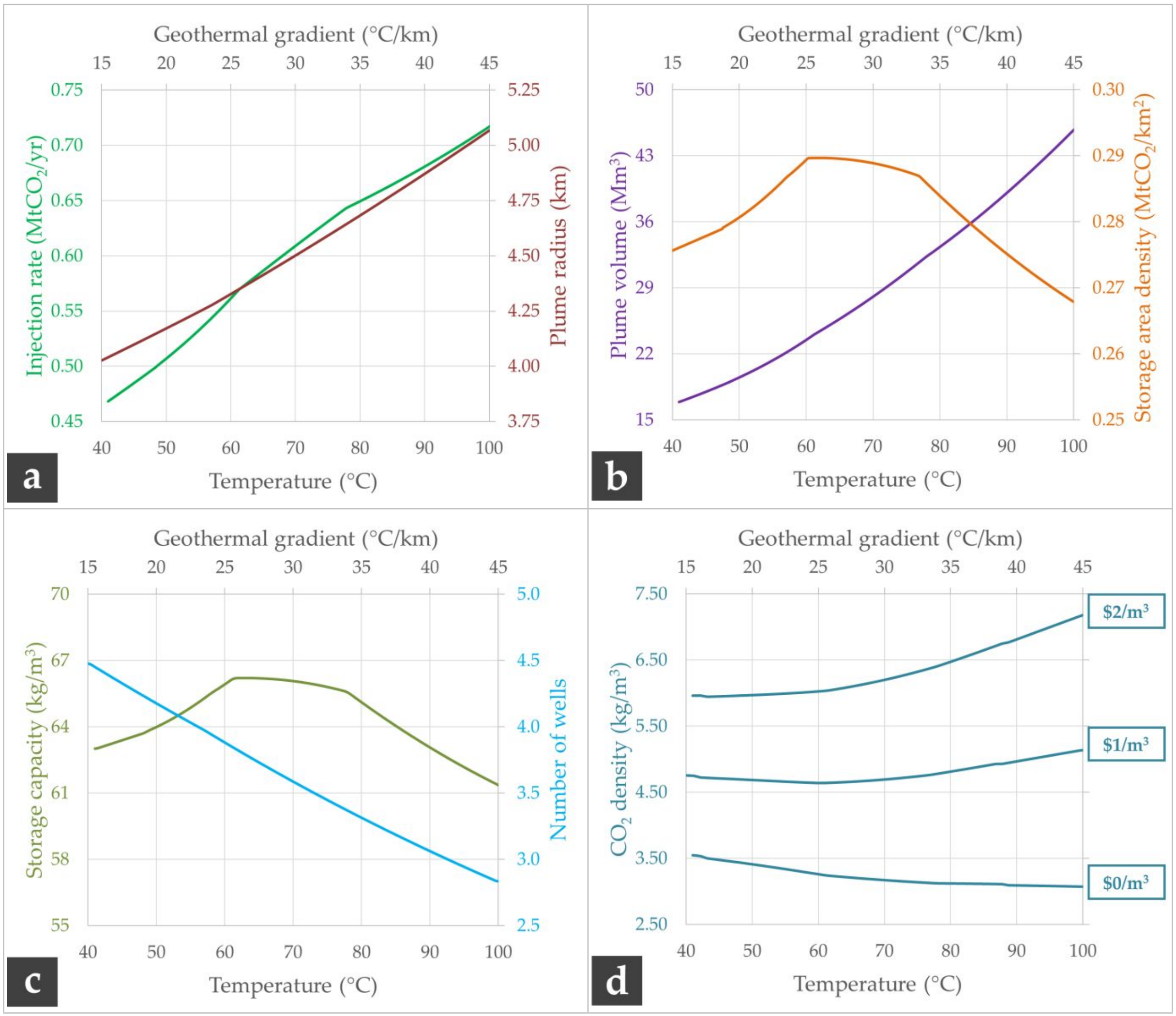

Figure 8: Impact of geothermal gradient on reservoir storage capacity and number of wells used (a) and CO_2 injection/storage costs (b). Geothermal gradient ranges between 15°C/km and 45°C/km while depth (2000 m), thickness (15 m), permeability (20 mD), and porosity (0.2) are held constant. CO_2 injection rate ranges between 0.5 and 0.75 $MtCO_2$/yr (i.e., does not reach the 1 $MtCO_2$/yr cap). For the injection/storage costs (b), three cost curves are shown with brine treatment/disposal costs ranging from \$0/tCO_2 to \$2/tCO_2.

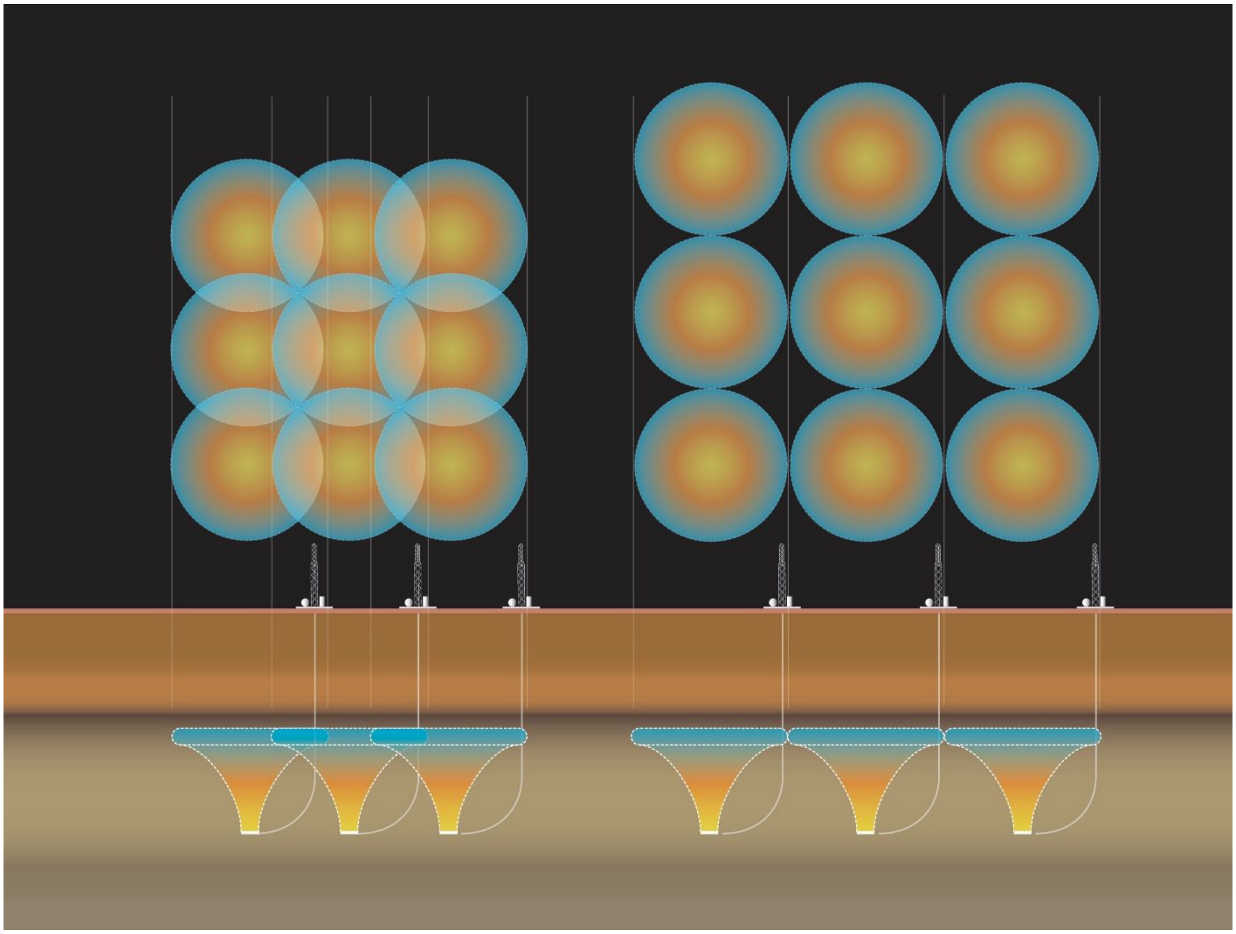

Figure 9: Conceptualization of overlapping plumes.

592

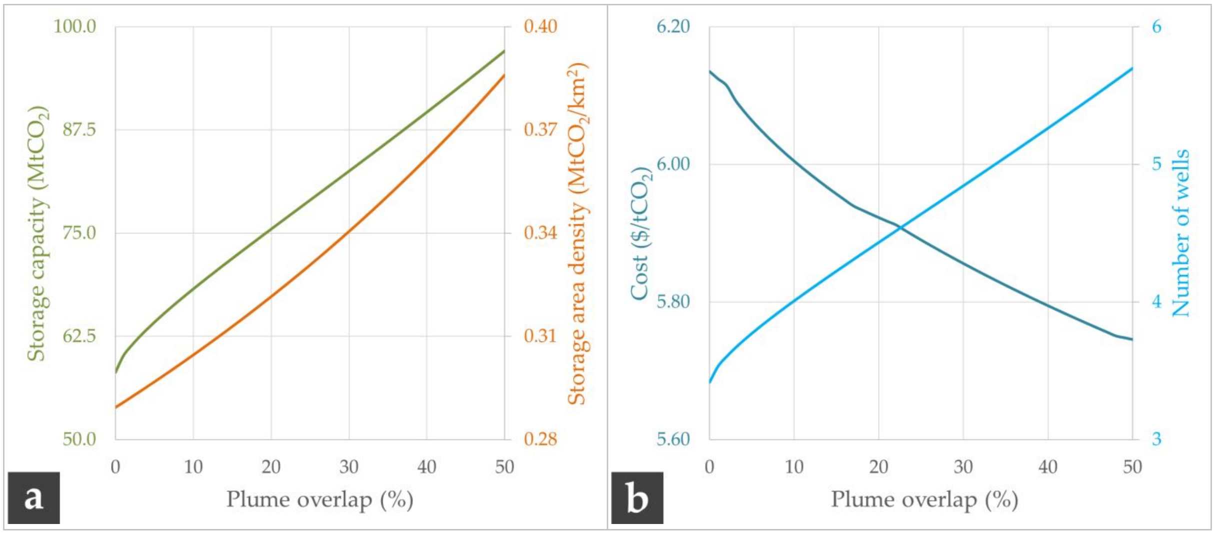

Figure 10: Impact of overlapping plumes (ranging from 0 to 50%) on storage capacity and storage area density (a) and cost and number of wells (b). While plume overlap ranges between 0 to 50%, depth (2000 m), thickness (15 m), permeability (20 mD), porosity (0.2), and geothermal gradient (25°C/km) are held constant. Wells have to be arranged in a square pattern (not the default hexagonal) in *SCO_2T* to allow the plume overlapping function.

593

8.0 REFERENCES

1. Kolster, C.; Masnadi, M. S.; Krevor, S.; Mac Dowell, N.; Brandt, A. R., CO_2 enhanced oil recovery: a catalyst for gigatonne-scale carbon capture and storage deployment? *Energy & Environmental Science* **2017,** *10*, (12), 2594-2608.
2. Chen, B.; Pawar, R. J., Characterization of CO_2 storage and enhanced oil recovery in residual oil zones. *Energy* **2019,** *183*, 291-304.
3. Lake, L. W.; Lotfollahi, M.; Bryant, S. L., CO_2 Enhanced Oil Recovery Experience and its Messages for CO_2 Storage. In *Science of Carbon Storage in Deep Saline Formations*, Elsevier: **2019**; pp 15-31.
4. Boot-Handford, M. E.; Abanades, J. C.; Anthony, E. J.; Blunt, M. J.; Brandani, S.; Mac Dowell, N.; Fernández, J. R.; Ferrari, M.-C.; Gross, R.; Hallett, J. P., Carbon capture and storage update. *Energy & Environmental Science* **2014,** *7*, (1), 130-189.
5. Heuberger, C. F.; Staffell, I.; Shah, N.; Mac Dowell, N., Quantifying the value of CCS for the future electricity system. *Energy & Environmental Science* **2016,** *9*, (8), 2497-2510.
6. Farhat, K.; Benson, S. M., A technical assessment of CO_2 Interim Storage in deep saline aquifers. *International Journal of Greenhouse Gas Control* **2013,** *15*, 200-212.
7. Chen, B.; Harp, D. R.; Lin, Y.; Keating, E. H.; Pawar, R. J., Geologic CO_2 sequestration monitoring design: A machine learning and uncertainty quantification based approach. *Applied Energy* **2018,** *225*, 332-345.
8. Teng, Y.; Zhang, D., Long-term viability of carbon sequestration in deep-sea sediments. *Science Advances* **2018,** *4*, (7), eaao6588.
9. Middleton, R. S.; Carey, J. W.; Currier, R. P.; Hyman, J. D.; Kang, Q.; Karra, S.; Jiménez-Martínez, J.; Porter, M. L.; Viswanathan, H. S., Shale gas and non-aqueous fracturing fluids: Opportunities and challenges for supercritical CO_2. *Applied Energy* **2015,** *147*, 500-509.
10. Celia, M. A.; Bachu, S.; Nordbotten, J.; Bandilla, K., Status of CO_2 storage in deep saline aquifers with emphasis on modeling approaches and practical simulations. *Water Resources Research* **2015,** *51*, (9), 6846-6892.
11. Benson, S. M., Negative-emissions insurance. *Science* **2014,** *344*, (6191), 1431-1431.
12. Fajardy, M.; Mac Dowell, N., Can BECCS deliver sustainable and resource efficient negative emissions? *Energy & Environmental Science* **2017,** *10*, (6), 1389-1426.
13. Fajardy, M.; Mac Dowell, N., The energy return on investment of BECCS: is BECCS a threat to energy security? *Energy & Environmental Science* **2018,** *11*, (6), 1581-1594.
14. Kumar, A.; Madden, D. G.; Lusi, M.; Chen, K. J.; Daniels, E. A.; Curtin, T.; Perry IV, J. J.; Zaworotko, M. J., Direct air capture of CO_2 by physisorbent materials. *Angewandte Chemie International Edition* **2015,** *54*, (48), 14372-14377.
15. Sanz-Perez, E. S.; Murdock, C. R.; Didas, S. A.; Jones, C. W., Direct capture of CO_2 from ambient air. *Chemical Reviews* **2016,** *116*, (19), 11840-11876.
16. Wilcox, J.; Psarras, P. C.; Liguori, S., Assessment of reasonable opportunities for direct air capture. *Environmental Research Letters* **2017,** *12*, (6), 065001.
17. de Coninck, H.; Benson, S. M., Carbon dioxide capture and storage: issues and prospects. *Annual Review of Environment and Resources* **2014,** *39*, 243-270.

18. Edwards, R. W.; Celia, M. A., Infrastructure to enable deployment of carbon capture, utilization, and storage in the United States. *Proceedings of the National Academy of Sciences* **2018,** *115*, (38), E8815-E8824.

19. Galan-Martin, A.; Pozo, C.; Azapagic, A.; Grossmann, I.; Mac Dowell, N.; Guillén-Gosálbez, G., Time for global action: an optimised cooperative approach towards effective climate change mitigation. *Energy & Environmental Science* **2018,** *11*, (3), 572-581.

20. Szulczewski, M. L.; MacMinn, C. W.; Herzog, H. J.; Juanes, R., Lifetime of carbon capture and storage as a climate-change mitigation technology. *Proceedings of the National Academy of Sciences* **2012,** *109*, (14), 5185-5189.

21. Middleton, R. S.; Levine, J. S.; Bielicki, J. M.; Viswanathan, H. S.; Carey, J. W.; Stauffer, P. H., Jumpstarting commercial-scale CO_2 capture and storage with ethylene production and enhanced oil recovery in the US Gulf. *Greenhouse Gases: Science and Technology* **2015,** *5*, (3), 241-253.

22. Mohlin, K.; Bi, A.; Brooks, S.; Camuzeaux, J.; Stoerk, T., Turning the corner on US power sector CO_2 emissions—a 1990–2015 state level analysis. *Environmental Research Letters* **2019,** *14*, (8), 084049.

23. Esposito, R. A.; Kuuskraa, V. A.; Rossman, C. G.; Corser, M. M., Reconsidering CCS in the US fossil‐fuel fired electricity industry under section 45Q tax credits. *Greenhouse Gases: Science and Technology* **2019**.

24. Middleton, R. S.; Keating, G. N.; Stauffer, P. H.; Jordan, A. B.; Viswanathan, H. S.; Kang, Q. J.; Carey, J. W.; Mulkey, M. L.; Sullivan, E. J.; Chu, S. P.; Esposito, R.; Meckel, T. A., The cross-scale science of CO_2 capture and storage: from pore scale to regional scale. *Energy & Environmental Science* **2012,** *5*, (6), 7328-7345.

25. Rogelj, J.; Shindell, D.; Jiang, K.; Fifita, S.; Forster, P.; Ginzburg, V.; Handa, C.; Kheshgi, H.; Kobayashi, S.; Kriegler, E., Mitigation pathways compatible with 1.5 C in the context of sustainable development. **2018**.

26. Metz, B.; Davidson, O.; De Coninck, H.; Loos, M.; Meyer, L. *IPCC special report on carbon dioxide capture and storage*; **2005**.

27. Coleman, J. L.; Cahan, S. M., *Preliminary catalog of the sedimentary basins of the United States*. US Department of the Interior, US Geological Survey: **2012**.

28. NETL NATCARB Atlas. https://www.netl.doe.gov/coal/carbon-storage/strategic-program-support/natcarb-atlas (last accessed August, **2019**).

29. Runkel, A. C.; Miller, J. F.; McKay, R. M.; Palmer, A. R.; Taylor, J. F., High-resolution sequence stratigraphy of lower Paleozoic sheet sandstones in central North America: The role of special conditions of cratonic interiors in development of stratal architecture. *Geological Society of America Bulletin* **2007,** *119*, (7-8), 860-881.

30. Warwick, P. D.; Blondes, M.; Brennan, S.; Buursink, M.; Cahan, S.; Coleman, J. L.; Corum, M.; Covault, J.; Craddock, W.; DeVera, C., National assessment of geologic carbon dioxide storage resources—Results. *US Geol. Surv. Circ* **2013,** *1386*, 41.

31. Buscheck, T. A.; Sun, Y.; Chen, M.; Hao, Y.; Wolery, T. J.; Bourcier, W. L.; Court, B.; Celia, M. A.; Friedmann, S. J.; Aines, R. D., Active CO_2 reservoir management for carbon storage: Analysis of operational strategies to relieve pressure buildup and improve injectivity. *International Journal of Greenhouse Gas Control* **2012,** *6*, 230-245.

32. Buscheck, T. A.; White, J. A.; Carroll, S. A.; Bielicki, J. M.; Aines, R. D., Managing geologic CO 2 storage with pre-injection brine production: a strategy evaluated with a model of CO 2 injection at Snøhvit. *Energy & Environmental Science* **2016,** *9*, (4), 1504-1512.

33. Buscheck, T. A.; Bielicki, J. M.; White, J. A.; Sun, Y.; Hao, Y.; Bourcier, W. L.; Carroll, S. A.; Aines, R. D., Pre-injection brine production in CO_2 storage reservoirs: An approach to augment the development, operation, and performance of CCS while generating water. *International Journal of Greenhouse Gas Control* **2016,** *54*, 499-512.

34. Sullivan, E. J.; Chu, S.; Stauffer, P. H.; Middleton, R. S.; Pawar, R. J., A method and cost model for treatment of water extracted during geologic CO_2 storage. *International Journal of Greenhouse Gas Control* **2013,** *12*, (0), 372-381.

35. Middleton, R. S.; Chen, B.; Harp, D. R.; Kammer, R. M.; Ogland-Hand, J. D.; Bielicki, J. M.; Clarens, A. F.; Currier, R. P.; Ellett, K. M.; Hoover, B. A.; McFarlane, D. N.; Pawar, R. J.; Stauffer, P. H.; Viswanathan, H. S.; Yaw, S. P., Great *SCO_2T*! Rapid tool for carbon sequestration science, engineering, and economics. *Applied Computing and Geosciences* **2020,** *7*, 100035.

36. McCoy, S.; Rubin, E., Models of CO_2 transport and storage costs and their importance in CCS cost estimates. **2005**, In Proceedings of The Fourth Annual Conference on Carbon Capture and Sequestration, DOE/NETL.

37. Stauffer, P. H.; Viswanathan, H.; Pawar, R. J.; Klasky, M. L.; Guthrie, G. D., *CO_2-PENS*: A CO_2 sequestration systems model supporting risk-based decisions. **2006**, Proceedings of the 16th International Conference on Computational Methods in Water Resources.

38. Stauffer, P. H.; Viswanathan, H. S.; Pawar, R. J.; Guthrie, G. D., A system model for geologic sequestration of carbon dioxide. *Environmental Science and Technology* **2009,** *43*, (3), 565-570.

39. Sifuentes, W. F.; Giddins, M. A.; Blunt, M. J., Modeling CO_2 Storage in Aquifers: Assessing the key contributors to uncertainty. *Offshore Europe* **2009**.

40. Wainwright, H. M.; Finsterle, S.; Zhou, Q.; Birkholzer, J. T., Modeling the performance of large-scale CO_2 storage systems: a comparison of different sensitivity analysis methods. *International Journal of Greenhouse Gas Control* **2013,** *17*, 189-205.

41. Metcalfe, R.; Bond, A.; Maul, P.; Paulley, A., Whole-system process modelling of CO_2 storage and its application to the In Salah CO_2 storage site, Algeria. *Energy Procedia* **2013,** *37*, 3859-3866.

42. Dai, Z.; Viswanathan, H.; Middleton, R.; Pan, F.; Ampomah, W.; Yang, C.; Jia, W.; Xiao, T.; Lee, S.-Y.; McPherson, B., CO_2 accounting and risk analysis for CO_2 sequestration at enhanced oil recovery sites. *Environmental Science & Technology* **2016,** *50*, (14), 7546-7554.

43. Dai, Z.; Viswanathan, H.; Fessenden-Rahn, J.; Middleton, R.; Pan, F.; Jia, W.; Lee, S.-Y.; McPherson, B.; Ampomah, W.; Grigg, R., Uncertainty Quantification for CO_2 Sequestration and Enhanced Oil Recovery. *Energy Procedia* **2014,** *63*, 7685-7693.

44. Zhang, Y.; Oldenburg, C. M.; Finsterle, S.; Bodvarsson, G. S., System-level modeling for economic evaluation of geological CO_2 storage in gas reservoirs. *Energy Conversion and Management* **2007,** *48*, (6), 1827-1833.

45. Middleton, R. S.; Bielicki, J. M., A scalable infrastructure model for carbon capture and storage: *SimCCS*. *Energy Policy* **2009,** *37*, (3), 1052-1060.

46. Middleton, R. S.; Yaw, S. P.; Hoover, B. A.; Ellett, K. M., *SimCCS*: An open-source tool for optimizing CO_2 capture, transport, and storage infrastructure. *Environmental Modelling & Software* **2020,** *124*, 104560.

47. Zyvoloski, G. A.; Robinson, B. A.; Dash, Z. V.; Trease, L. L. *Summary of the models and methods for the FEHM application-A finite-element heat- and mass-transfer code*; http://fehm.lanl.gov **1997**.

48. Zyvoloski, G. A. *FEHM: A control volume finite element code for simulating subsurface multi-phase multi-fluid heat and mass transfer*; http://fehm.lanl.gov **2007**.

49. Zyvoloski, G. A.; Robinson, B. A.; Dash, Z. V.; Kelkar, S.; Viswanathan, H. S.; Pawar, R. J.; Stauffer, P. H.; Miller, T. A.; Chu, S., Software users manual (UM) for the FEHM application version 3.1-3X. *Los Alamos National Laboratory, Los Alamos* **2011**.

50. Chen, B.; Harp, D. R.; Pawar, R. J.; Stauffer, P. H.; Viswanathan, H. S.; Middleton, R. S., Frankenstein's ROMster: Avoiding pitfalls of reduced-order model development. *International Journal of Greenhouse Gas Control* **2020,** *93*, 102892.

51. USEPA *Geologic CO_2 Sequestration Technology and Cost Analysis*; http://water.epa.gov/type/groundwater/uic/class6/upload/geologicCO2sequestrationtechnologyandcostanalysisnov2010.pdf **2010**.

52. Grant, T.; Morgan, D. *FE/NETL CO_2 Saline Storage Cost Model (2017): User's Manual*; **2017**.

53. Nordbotten, J. M.; Celia, M. A.; Bachu, S., Injection and storage of CO_2 in deep saline aquifers: Analytical solution for CO_2 plume evolution during injection. *Transport in Porous Media* **2005,** *58*, 339-360.

54. Middleton, R. S.; Yaw, S., The cost of getting CCS wrong: Uncertainty, infrastructure design, and stranded CO_2. *International Journal of Greenhouse Gas Control* **2018,** *70*, 1-11.

55. Global CCS Institute ***2019 Global Status of CCS***; https://www.globalccsinstitute.com/wp-content/uploads/2019/12/GCC_GLOBAL_STATUS_REPORT_2019.pdf **2019**.

IMPACT

CO_2 capture and storage (CCS) is a critical technology for energy, the environment, and economic security. CCS is part of every clean energy pathway that limits global warming to 2°C and will change how we produce and consume energy. To have a meaningful impact, CCS will have to be deployed on a massive scale, potentially capturing and storing billions of tonnes of CO_2 each year around the globe. Identifying sites that can safely and cost-effectively store this amount of CO_2 relies on being able to quickly and accurately understand what large-scale CO_2 injection and storage. Our study focused on this critical research gap. We used the *SCO₂T* sequestration tool to explore the effect of key geologic characteristics (such as reservoir depth, thickness, permeability, porosity, and temperature) and operational decisions on the engineering and economics of carbon sequestration. We were able to show new and unintuitive effects that will be both important for fundamental environmental science research as well as understanding how we can meet climate and energy targets.